SANDIA REPORT

SAND89-8718
Unlimited Release
Printed January 1990

Hydrogen Effects on Fracture Toughness of Ti-6Al-4V Determined by a Steadily Growing Stable Crack

Submitted to Proceedings of the Fourth International Conference on Hydrogen Effects on Material Behavior

J. P. Lucas

Prepared by
Sandia National Laboratories
Albuquerque, New Mexico 87185 and Livermore, California 94551
for the United States Department of Energy
under Contract DE-AC04-76DP00789

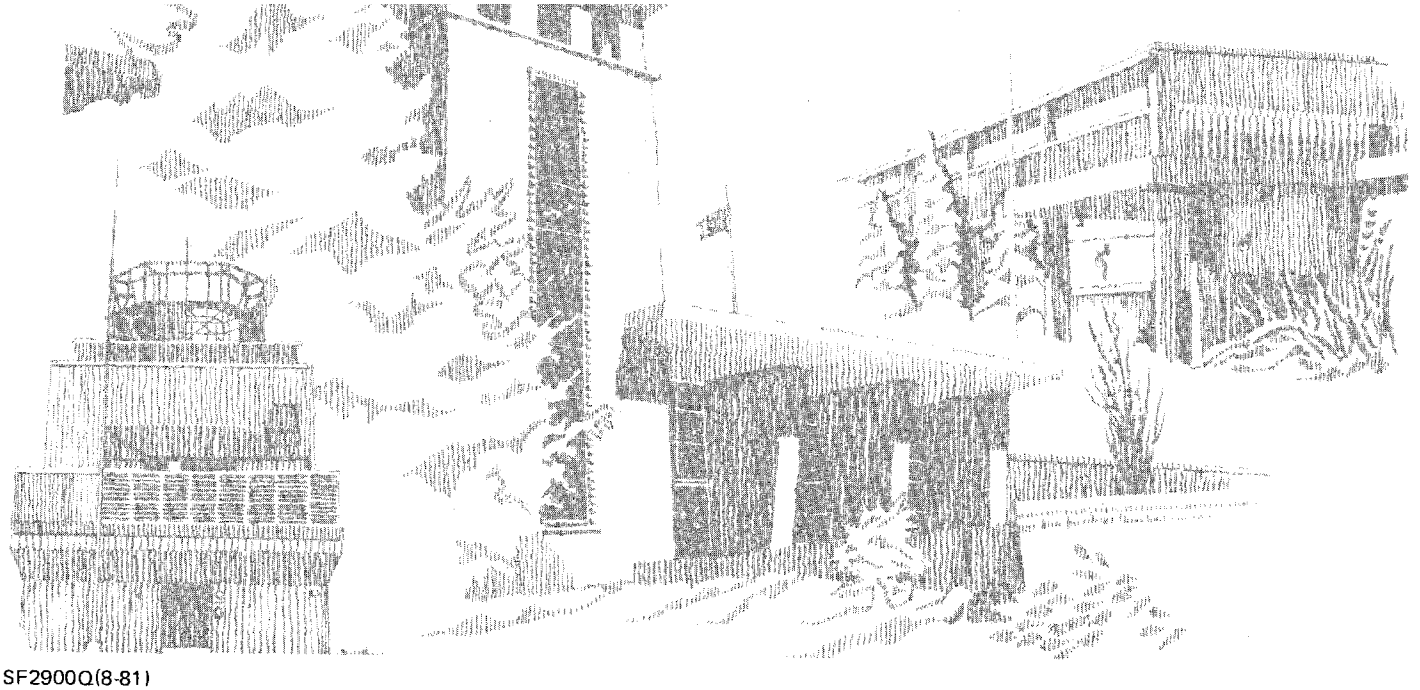

Issued by Sandia National Laboratories, operated for the United States Department of Energy by Sandia Corporation.

SAND89-8718
Unlimited Release
Printed January 1990

HYDROGEN EFFECTS ON FRACTURE TOUGHNESS OF Ti-6Al-4V DETERMINED BY A STEADILY GROWING STABLE CRACK

J. P. Lucas
Joining and Physical Metallurgy Division
Sandia National Laboratories
Livermore, California 94551-0969

Abstract

Many investigations have been conducted on the effect of hydrogen on crack initiation fracture toughness. In contrast, far less work has been done on the effect of hydrogen on fracture toughness determined by a steadily growing stable crack. In this study, the effect of hydrogen concentration on fracture toughness was determined by using a specimen in which the fracture toughness was measured by a steadily growing stable crack. Specifically, a nonconventional test specimen, a chevron notched short bar specimen (CNSB), was used. Internal hydrogen effects on fracture toughness were determined for an α–β titanium alloy, Ti-6Al-4V, with hydrogen content ranging from 10 to 200 wppm. The CNSB fracture toughness results exhibited a marked effect of hydrogen concentration. The fracture toughness determined at 10 wppm hydrogen was nearly twice as high as that determined at 200 wppm hydrogen. Results showed a steep increase in fracture toughness for material with hydrogen concentration < 50 wppm. Essentially, no change in fracture was observed for material of hydrogen content from 50 to 200 wppm. There was no observable difference in fracture surface morphological character that was commensurate with the hydrogen-induced change in CNSB fracture toughness. Regardless of hydrogen content, fracture was characterized predominantly by a ductile failure mode with few isolated cleavage facets. Despite fractographic similitude, acoustical emission (AE) results did suggest a difference in microfracture processes of Ti-6Al-4V alloy containing low and high hydrogen concentration levels. An appreciable difference existed in AE energy and AE events count signals for material of 10 and 200 wppm hydrogen that was tested in the stable crack growth regime. The AE results were used to assess the influence of hydrogen concentration crack tip fracture mechanisms.

ACKNOWLEDGEMENTS

I wish to acknowledge the support of N. R. Moody for his assistance in hydrogen-charging of materials. Thanks are also extended to T. Sage, B. Brown, A. Gardea, and L. Cruz. This work was supported by DOE through contract DE-AC04-76DP00789.

TABLE OF CONTENTS

	Page
Acknowledgments	5
Introduction	9
Materials and Experimental Procedures	10
Materials and Microstructure	10
Tensile and Fracture Toughness Methods	13
Acoustic Emission	15
Results and Discussion	15
Tensile	15
Fracture Toughness	19
AE Fracture Interpretation	23
Summary and Conclusions	29
References	32
Tables	
Table I	11
Table II	11
Table III	18
Table IV	22
Figures	
1	12
2	14
3	16
4	17
5	20
6	21
7	24
8	25
9	26
10	27
11	28
12	30
13	31
Distribution	34

HYDROGEN EFFECTS ON FRACTURE TOUGHNESS OF Ti-6Al-4V DETERMINED BY A STEADILY GROWING STABLE CRACK

Introduction

The effects of hydrogen on tensile and fracture properties of α–β titanium alloys have been well documented by a number of investigations [1-10]. For α–β titanium alloys, earlier investigations showed tensile properties were affected only slightly by hydrogen concentration. Hoeg et al. showed that the tensile properties of Ti-6Al-4V were not seriously degraded by internal hydrogen up to 500 ppm [1]. Similar findings were made by Enjo and Kuroda [2] that the internal hydrogen concentration could reach 1500 ppm in Ti-6Al-4V alloy before tensile properties dramatically decreased. These investigations [1-3] also suggested that high internal hydrogen concentrations were required for embrittlement to occur in smooth gage and mildly notched tensile specimens. The susceptibility of α and α–β titanium alloys to hydrogen embrittlement was also dependent on microstructure and strain rate [4]. For cracked and acutely notched materials under an applied load, susceptibility to hydrogen embrittlement occurs at substantially lower internal hydrogen concentrations. Although some controversy still exists, two widely held views endure regarding hydrogen susceptibility of flawed specimens. One view suggests that the crack tip is supersaturated with hydrogen resulting from strain gradients in the crack tip region, which subsequently precipitate hydrides at the α–β interface to assist in the crack initiation and growth [5,6]. The other simply suggests that hydrogen remains in solution and embrittlement occurs in the material when the hydrogen concentration is sufficient to reduce the cohesive strength [7]. Meyn [8], for example, concluded that hydride cracking was not a crack initiation mechanism in Ti-6Al-4V alloy, but rather, cracking initiated within the α grain and/or the α/β interface ahead of the main crack. He also reported that the characteristic fracture mode was cleavage on crystallographic planes 12 to 15 degrees from the $\{0001\}_\alpha$ and the $\{0001\}_\alpha$ itself. Williams showed that sustained-load subcritical crack growth proceeded in α–β titanium alloys having hydrogen concentrations of about 10 ppm in a hydrogen-producing environment [9]. Because subcritical cracking occurred in Ti-4Al-3Mo-1V at very low hydrogen levels, fracture was attributed to a creep phenomenon in which failure occurred upon achieving a critical creep strain. It was suggested that subcritical crack growth resulted by a combination of microfracture mechanisms involving α–β interfacial separation, microporosity linking in the β phase, and cleavage in the α phase. Under slow bend conditions, H-charged notched bars fractured in high vacuum were shown to fail exclusively by cleavage in the α phase and ductile rupture in the β phase of Ti-6Al-6V-2Sn material [10]. Unlike the charged material, it was shown by Peterson et. al. [10] that the

uncharged material fractured by a ductile transgranular mode. Most investigations mentioned thus far appear to have a common link in regards to the effect of hydrogen of fracture in α–β titanium alloys. That is, under sustained loading in which ample time is available for hydrogen diffusion to take place, fracture initiated either by cleavage in the α phase or by cracking of hydrides that have precipitated at the α/β interface. In these investigations [6,7,9], the effect of hydrogen on fracture toughness was assessed by conducting tests involving either crack initiation or crack arrest.

Very little information, however, is available that demonstrates the effect of hydrogen on fracture toughness for steadily-growing stable cracks. In this study the effect of hydrogen on fracture toughness has been determined by using a specimen in which fracture toughness is measured by a steadily-growing stable crack. Hydrogen-induced effects on fracture toughness and tensile properties were determined for Ti-6Al-4V with hydrogen concentrations ranging from 10 to 200 wppm. Specifically, a nonconventional test specimen (chevron-notched short bar, CNSB) was used to determine fracture toughness. Also, acoustic emission (AE) data were acquired during fracture toughness testing. The AE data were used in the interpretation of fracture mechanisms associated with fracture toughness in α–β titanium alloy as a function of hydrogen concentration. Further motivation for this investigation was provided by an interest in assessing the feasibility of using small CNSB specimens for determining fracture toughness. Also, there was a strong interest in determining whether the CNSB test method would be capable of differentiating between subtle as well as gross changes of H-induced fracture in an α–β titanium alloy.

Materials and Experimental Procedures

Materials and Microstructure

The microstructure of α–β Ti-6Al-4V alloy in this study is characterized by elongated α grains with some transformed grain boundary β phase. The alloy chemical composition is listed in Table I. A consistent microstructure was maintained for both the H-charged and uncharged specimens. The microstructural consistency is clearly shown in Figs. 1A-1D for materials containing 10, 50, 115, and 200 wppm hydrogen respectively. It was essential that microstructural consistency be maintained so that the hydrogen-induced effects on the mechanical properties, in particular the fracture toughness, could be determined unambiguously without the clouding influence of microstructure variation. The samples were gas-phase charged with hydrogen to concentrations up to 200 wppm using a Sieverts apparatus. The

TABLE I						
Composition (wt%)						
Al	V	Fe	O	C	N	Ti
5.8	3.8	0.3	0.2	0.1	0.05	Bal.

Table I. The nominal chemical composition is given in weight percent for Ti-6Al-4V alloy.

TABLE II		
Hydrogen (wppm)		Hydrogen Charging Parameters
10		Anealed 4h at 800 C in vacuum
25		Anealed 4h at 800 C in Ar
30		Anealed 4h at 800 C in Ar
50		Charged 4h at 800 C in hydrogen
60		Charged 4h at 800 C in hydrogen
115		Charged 4h at 800 C in hydrogen
200		Charged 4h at 800 C in hydrogen

Table II. The levels of hydrogen concentration and the charging conditions are listed for Ti-6Al-4V test specimens.

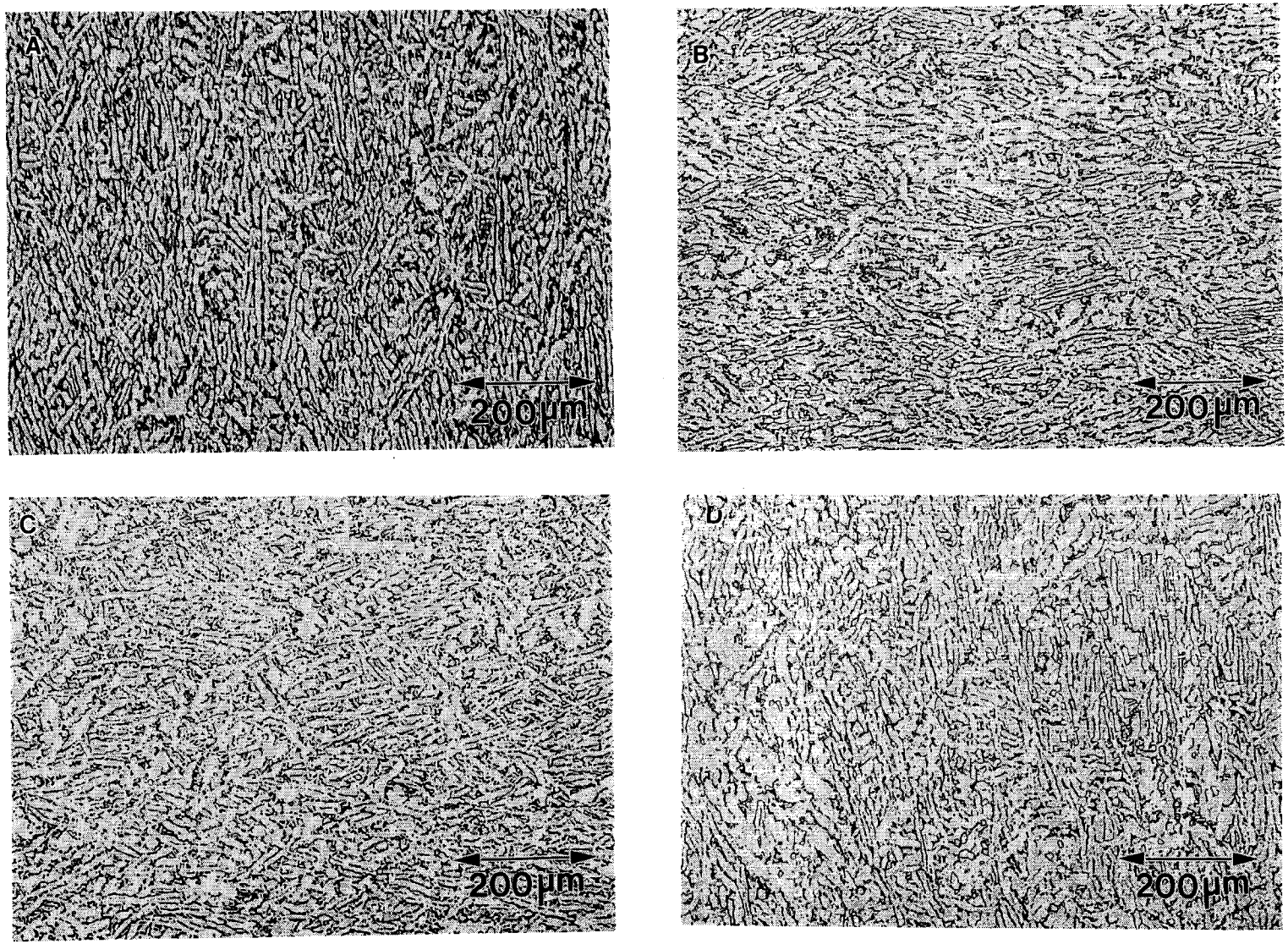

Fig. 1: The microstructures of Ti-6Al-4V alloys are shown for various hydrogen concentration levels; (A) 10 wppm, (B) 50 wppm, (C) 115 wppm and (D) 200 wppm.

hydrogen concentration levels and the hydrogen charging parameters are listed in Table II. Hydrogen charging procedures consisted of heating the samples to 800° C in vacuum at 10^{-5} Torr for 4 h during which time hydrogen gas was introduced into the furnace which was rapidly absorbed by the specimens. The four hour time duration at temperature ensured uniform distribution of internal hydrogen within the charged materials. Since the specimens were subsequently furnace cooled to room temperature, additional time was available for even further hydrogen homogenization within the material.

Tensile and Fracture Toughness Methods

Both tensile and short bar fracture toughness specimens were fabricated from the same bar stock material. Threaded tensile bars were fabricated with the following dimensions: gage length 25.4 mm , gage diameter 3.2 mm, and the overall length was 63.5 mm. The dimensions of the short bar specimen are given in Fig. 2. The length (W), the height (H) and the width (W) are 19.05 mm, 11.05 mm and 12.7 mm respectively. During testing, the axial alignment of tensile specimens was parallel to the extrusion direction of the bar stock material. Also, short bar specimens were oriented such that the crack propagation plane was aligned parallel to the bar stock extrusion direction. Uniaxial tension testing was conducted in ambient air at a strain rate (ε) of 3.3×10^{-4} sec^{-1} on an Instron® materials test system. During tensile testing in this strain rate regime, hydrogen effects are expected provided the material is sensitive to internal hydrogen [5,6]. Multiple tensile samples were tested at each hydrogen concentration level to ensure statistically credible results. Tensile strength, reduction-in-area (RA), and fracture strain (ε_f) data were obtained as a function of hydrogen concentration.

Fracture toughness (K_{ICSB}) data were obtained with a Terra-Tek Fractometer II® fracture toughness test system. Using the chevron notched short bar specimen, plane strain fracture toughness can be determined from the following expression:

$$K_{ICSB} = \left[\frac{(1+S)}{(1-S)}\right]^{1/2} \times \frac{A\Omega P_c}{B^{3/2}} \qquad (1)$$

where A is a constant for a fixed specimen geometry, Ω is a geometrical correction factor, P is the applied load, S is the plasticity factor, and B is the width of the specimen [11,12]. Again, statistically significant K_{ICSB} results were ensured by testing several short bar samples at each hydrogen concentration. Figure 2 schematically shows the short bar specimen used to determine fracture toughness. Fracture toughness tests were conducted in room air at 25° C.

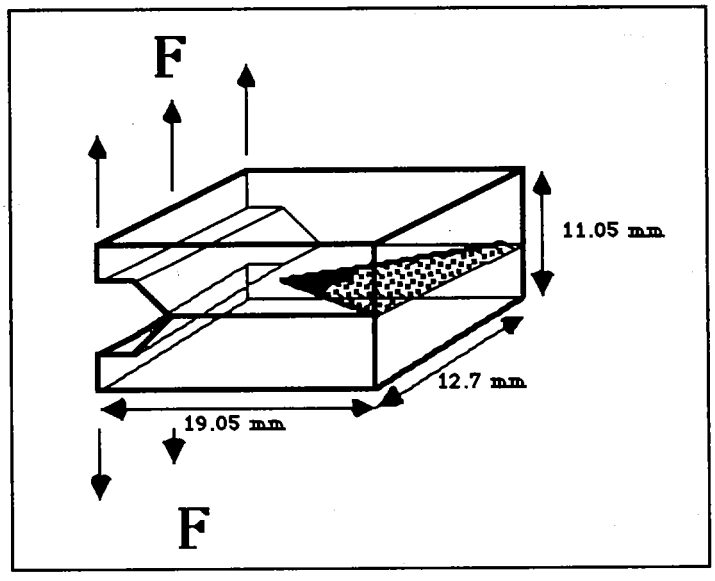

Fig. 2: A schematic diagram is shown of a CNSB specimen along with its dimensions.

The load-point displacement rate was 2.0 x 10^{-3} mm/sec. The CNSB specimen has advantages over conventional fracture toughness specimens (e.g., ASTM E-399) in that K_{ICSB} toughness values can be obtained with a smaller size specimen and conducting testing is remarkably simple. For similar thickness specimens, the volume of material used to fabricate the CNSB specimen is only about 10 percent of the volume of material used to fabricate for compact tension specimen, CTS. Furthermore, pre-fatigue cracking is not required. A sharp crack initiates at the apex of the chevron notch ligament which experiences a high stress intensity level upon applying a load to the specimen. Under constant load line displacement, the crack in the short bar specimen continues to grow, stably, under plane strain conditions until a critical crack length is reached. When this critical crack is reached, the fracture toughness (K_{ICSB}) is determined provided linear elastic fracture mechanics (LEFM) criteria are met. For sufficiently brittle materials, only the peak load is needed in order to determine K_{ICSB}. However, when the degree of crack tip plasticity is sufficient to violate LEFM criteria, a plasticity correction factor 's' is invoked in determining the fracture toughness value [11,12]. It is noted that the use of the plasticity correction factor is valid only when the plasticity at crack tip is small [12].

Acoustic Emissions

Acoustic emission (AE) data were obtained using a Physical Acoustic TM 4300 count analyzer. During fracture toughness testing, the AE output signal was detected with a PZT piezo-electric transducer with a resonance frequency of 150 kHz coupled to the short bar fracture toughness specimen. AE signals from the transducer were preamplified and processed through a band pass filter with a frequency range from 100-300kHz. The overall AE system gain was 46 dB. Apiezon M® coupling agent was used to improve coupling and transfer sensitivity between the specimen and the transducer. A constant coupling pressure was maintained between the transducer and specimen during all tests. This was achieved by holding the transducer in place by an opposing spring configuration as shown in Fig. 3. Using constant pressure coupling, AE data acquisition was more consistent.

Results and Discussion

Tensile

The tensile property results as a function of internal hydrogen concentration are shown in Fig. 4. Each data point plotted in Fig. 4 represents the average value of at least three tests at each hydrogen level. A compilation of all tensile data is listed in Table III. It is apparent that

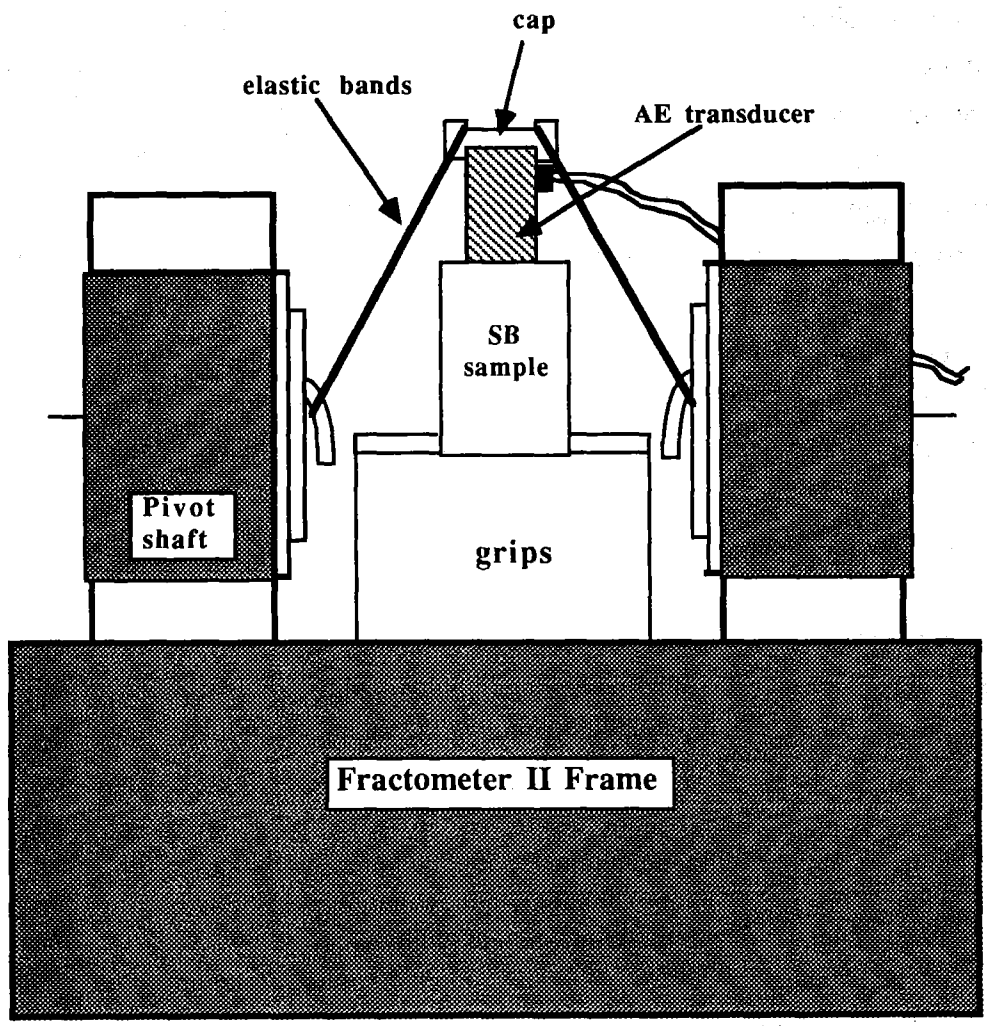

Fig. 3: A typical configuration of the AE transducer and CNSB specimen experimental test set up is illustrated .

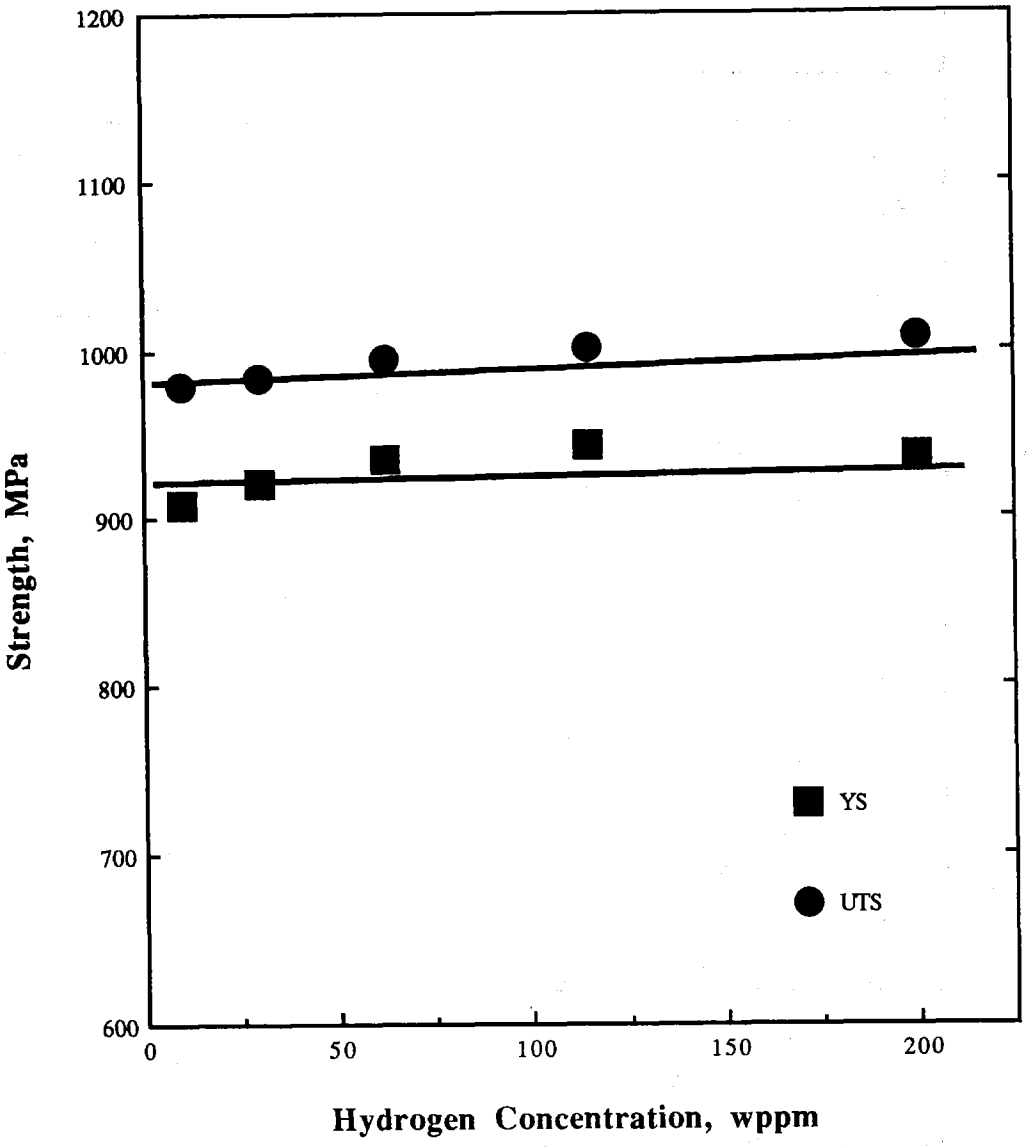

Fig. 4: The yield and ultimate strength data are shown as a function of hydrogen concentration.

TABLE III						
Mechanical Properties						
Hydrogen wppm	YS ksi	UTS ksi	YS MPa	UTS MPa	ef	%RA
10	132.3	142.2	912.87	981.18	18.6	41.5
10	131.4	140.8	906.66	971.52		
10	130.9	142.8	903.21	985.32		
30	133.5	142.4	921.15	982.56	20.4	39.5
30	131.3	142.8	905.97	985.32		
30	132.3	142.8	912.87	985.32		
62	133.5	142.4	921.2	982.56	20.8	43
62	134.8	144.8	930.12	999.12		
62	136.1	145.7	939.09	1005.33		
115	135.6	144.1	935.64	994.29	21.5	43.8
115	136.8	145.5	943.92	1003.95		
115	137.4	145.7	948.06	1005.33		
200	135.8	146.5	937	1010.85	20.8	41.5
200	136.5	147.8	941.85	1019.82		
200	134.8	143.4	930.12	989.46		

Table III. Tensile and ductility results are listed as a function of hydrogen concentration.

strength was not significantly affected by internal hydrogen, at least up to 200 wppm. The yield strength (σ_y) of the material at 10 wppm hydrogen was 910 MPa, while at 200 wppm hydrogen the σ_y increased slightly to 940 MPa. A similar trend was observed for the ultimate tensile strength (σ_T). Ductility and fracture strain (ε_f) results are plotted in Fig. 5 for various hydrogen concentrations. Ductility is not seriously affected by internal hydrogen over the range concentrations examined in this study. Previous investigations [1,2,6,13] showed similar trends in tensile properties for H-charged α–β titanium alloys. Pao [13] observed that hydrogen in solution between 50 and 500 wppm had no deleterious effects on the tensile properties on a similar near-α titanium alloys. Moreover, it was suggested [13] that internal hydrogen affected strength and ductility only when the hydrogen solubility limit was reached or when hydride precipitation occurred in the near-α titanium alloys. It appears that rather high concentrations are necessary to cause hydrogen-induced degradation of tensile properties in α–β titanium alloys. For example, the hydrogen solubility reached 1500 ppm before deleterious effects on the strength were observed in Ti-6Al-4V [2].

Fracture Toughness

There was a marked effect of hydrogen concentration on the short bar fracture toughness, K_{ICSB}. The effect of hydrogen on fracture toughness is shown in Fig. 6 where several data points are plotted at each hydrogen concentration level. Multiple tests conducted at each hydrogen concentration level showed little scatter in the experimental toughness data. Results for all fracture toughness tests conducted are listed in Table IV. Determining fracture toughness by the CNSB method is unique because the nature of crack tip propagation differs between the CNSB specimen and the CTS. Contrary to CTS in which fracture toughness is measured at crack initiation, the fracture toughness using the CNSB specimen is determined from a stably growing crack. The steadily-growing stable crack velocity was estimated to be about 1.5×10^{-2} mm/sec. Even though the CNSB method of determining fracture toughness differs considerably, comparison studies conducted in our laboratory exhibited remarkable agreement in fracture toughness results between conventional CTS and unconventional CNSB test specimens. An appreciable hydrogen effect was observed on short bar fracture toughness at hydrogen concentration levels <50 wppm. Below 50 wppm hydrogen, K_{ICSB} increased by nearly a factor of 2. However, at hydrogen levels greater than 50 wppm, K_{ICSB} was virtually constant exhibiting a limiting value with increasing H concentration. Similar trends of hydrogen effects on fracture toughness were observed by Meyn [8] and Williams [14] for Ti-6Al-4V alloy using wedge open loading (WOL) specimens [15]. Despite the substantial difference in fracture toughness results between materials of low and high hydrogen

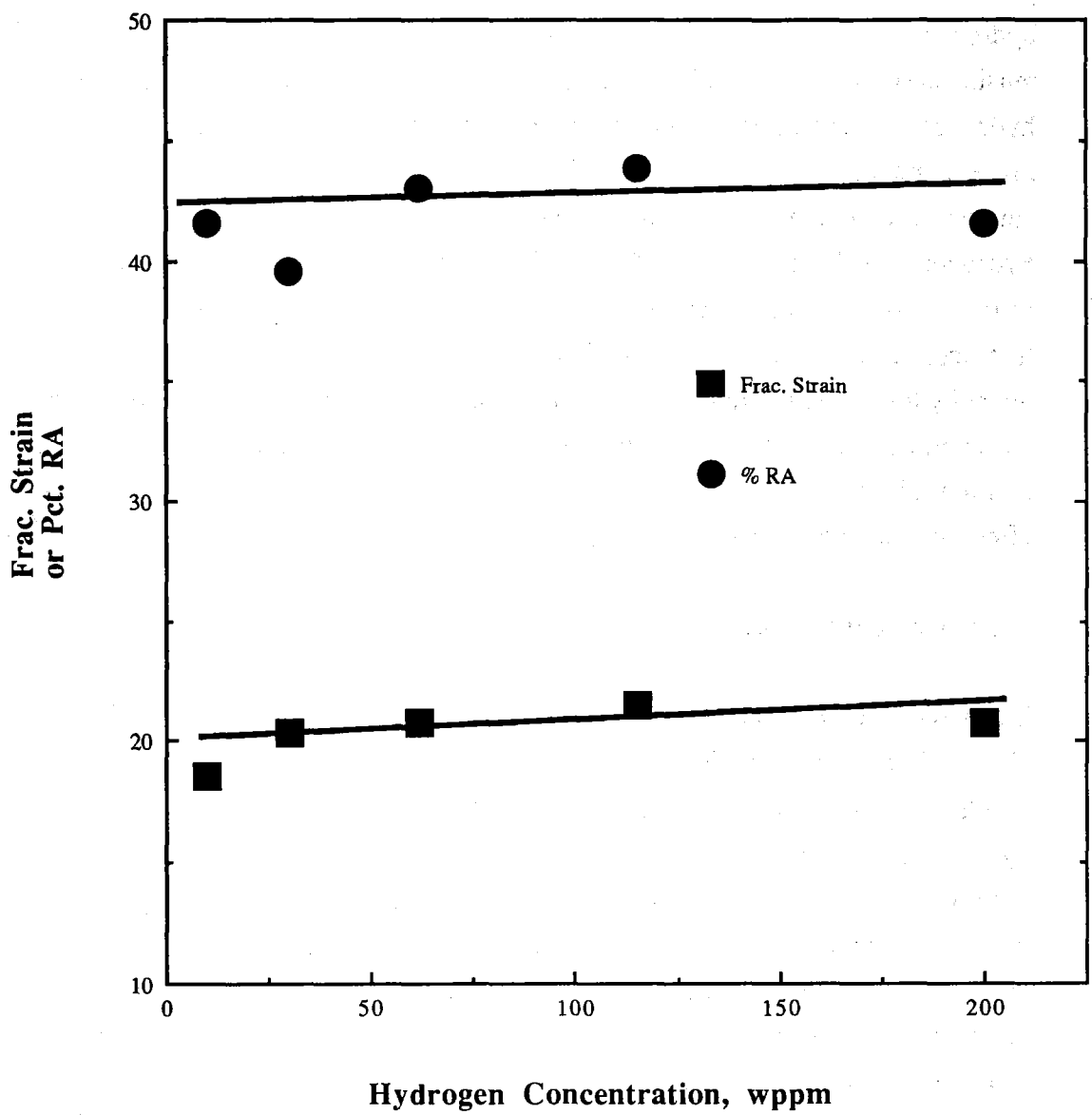

Fig. 5: Ductility data, RA and fracture strain, are exhibited as a function of hydrogen concentration.

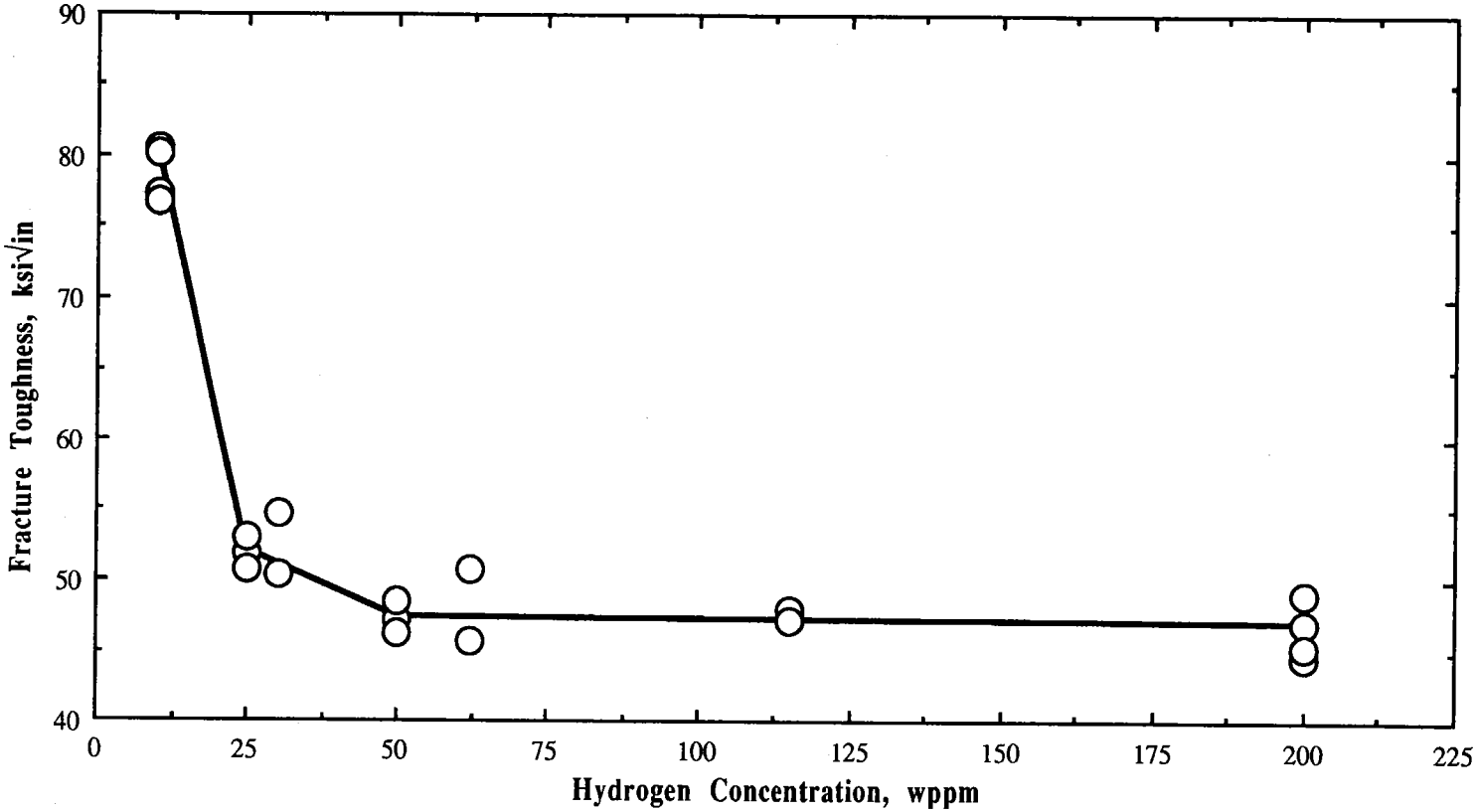

Fig. 6: The effect of hydrogen on CNSB fracture toughness is demonstrated for hydrogen levels ranging from 10 to 200 wppm .

TABLE IV		
Fracture Toughness		
Hydrogen wppm	K(ICSB) ksi$\sqrt{in}$	K(ICSB) MPa$\sqrt{m}$
10	77.30	84.26
10	76.80	83.71
10	80.50	87.75
10	80.20	87.42
25	51.98	56.66
25	53.00	57.77
25	50.80	55.37
30	54.70	59.62
30	50.30	54.83
50	47.20	51.45
50	46.30	50.47
50	48.50	52.87
62	50.80	55.37
62	45.70	49.81
115	48.00	52.32
115	47.10	51.34
200	44.60	48.61
200	45.30	49.38
200	46.90	51.12
200	45.20	49.27
200	49.15	53.57

Table IV. Mutilple tests data of fracture toughness are listed at various levels of hydrogen concentrations.

concentration levels, the microfracture surface appearance regardless of H-content was essentially the same. Figures 7A-7D show SEM micrographs of the α–β titanium alloys fracture surfaces at varying hydrogen concentration levels. Clearly, the fracture surface morphologies in Fig. 7 are virtually indistinguishable in general deformation character and fracture mode. Other investigators [8,14,16] have reported that the fracture mode was characteristically similar and the fracture surface morphology was unaffected by the level of internal hydrogen in Ti-6Al-4V. Primarily, fractography of all short bar samples tested exhibited a fracture mode characterized by ductile rupture and ligament tearing of the β phase with a few isolated quasi-cleaved facets in the α phase. Often times for materials with varying hydrogen concentrations, evidence of hydrogen-assisted fracture mechanisms is revealed by alternative fracture modes exhibited on the fracture surface. Hydrogen-induced alternative fracture modes were not seen on the fracture surface of either H-charged or uncharged Ti-6Al-4V alloys. Therefore, another diagnostic technique was used to probe for possible microfracture mechanisms involved in fracture toughness determination. AE monitoring was utilized during fracture toughness testing in order to acquire additional information which could be related to fracture mechanisms of H-charged Ti-6Al-4V.

AE Fracture Interpretation

Since the morphological character and the fracture surface appearance did not differ with hydrogen content, acoustic emission (AE) data profiles were used to help gain further insight into possible mechanisms of hydrogen assisted fracture processes. Acoustic emission data were obtained during short bar fracture toughness testing of the H-charged specimens. Despite the similarity in fracture surface morphology for hydrogen charged materials, major differences were observed in AE activity. This is shown in Fig. 8 where the fracture toughness is plotted along with the AE activity. Figure 8 indicates that the extent of emissions/COD is small for hydrogen-lean, high fracture toughness materials, while the extent of emissions/COD is significantly greater for hydrogen-rich, low fracture toughness materials. In previous investigations [17-22], AE was used to assess microfracture mechanisms in materials of both crack initiation and subcritical crack growth. Furthermore, most of these studies [18,20,21] have shown direct correlation between the degree of crack extension and the amount of AE activity. During fracture toughness testing of hydrogen charged Ti-6Al-4V alloy, a significant difference was observed in AE activity. In Figs. 9A and 9B the AE activity is exhibited coincidently with the load/displacement profile. The AE amplitude was significantly greater for the hydrogen-rich Ti-6Al-4V alloy during stable crack growth. The higher AE output for material with increased hydrogen concentration indicated that the elastic energy release per

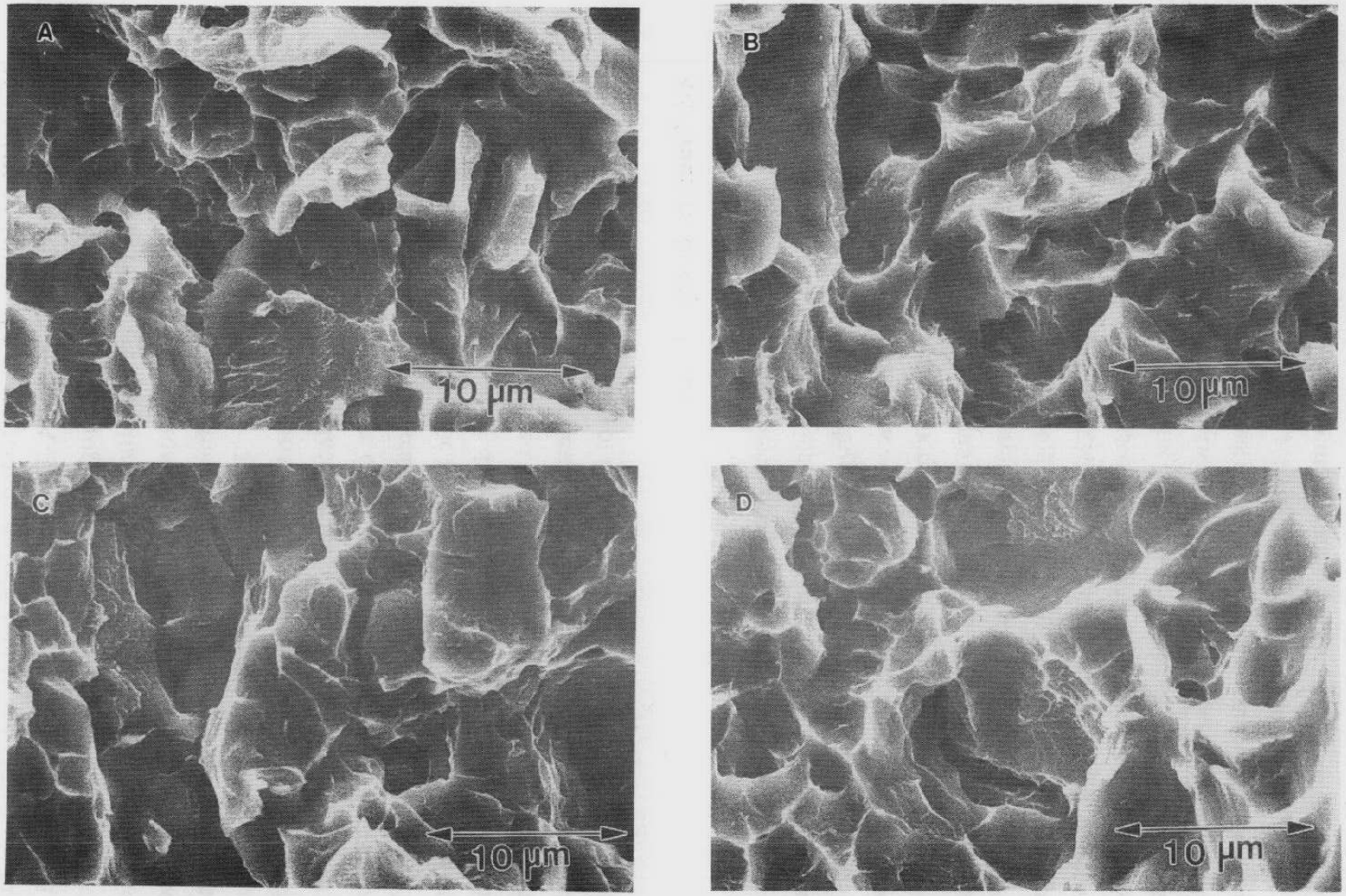

Fig. 7: SEM fractographs of Ti-6Al-4V material showed similar fracture surface morphological characteristics with varying hydrogen concentrations; (A) 10 wppm, (B) 25 wppm, (C) 50 wppm and (D) 200 wppm.

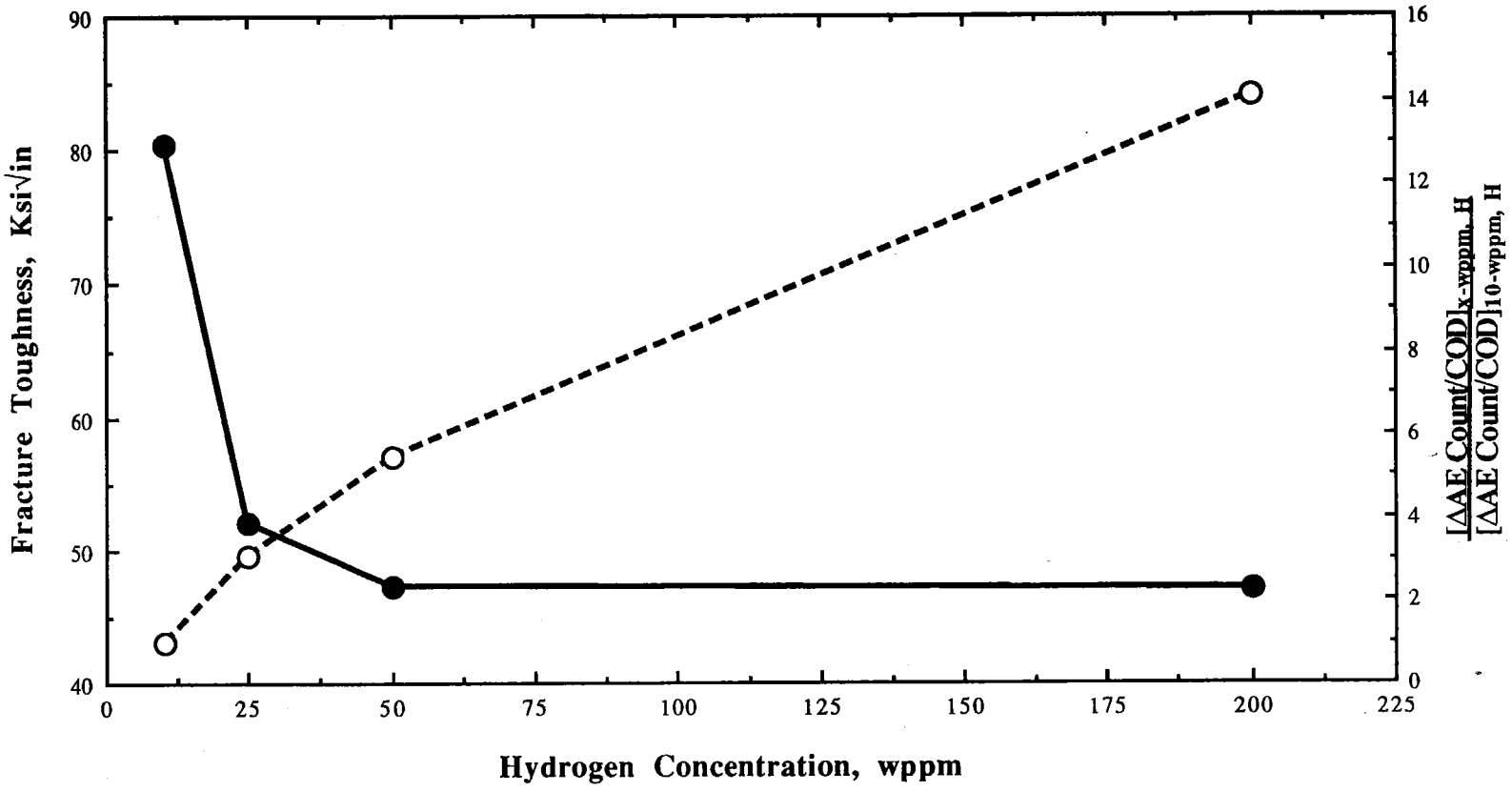

Fig. 8: The influence of hydrogen concentration on fracture toughness is shown. Also, the extent of acoustic emission activity increased as the hydrogen concentration increased.

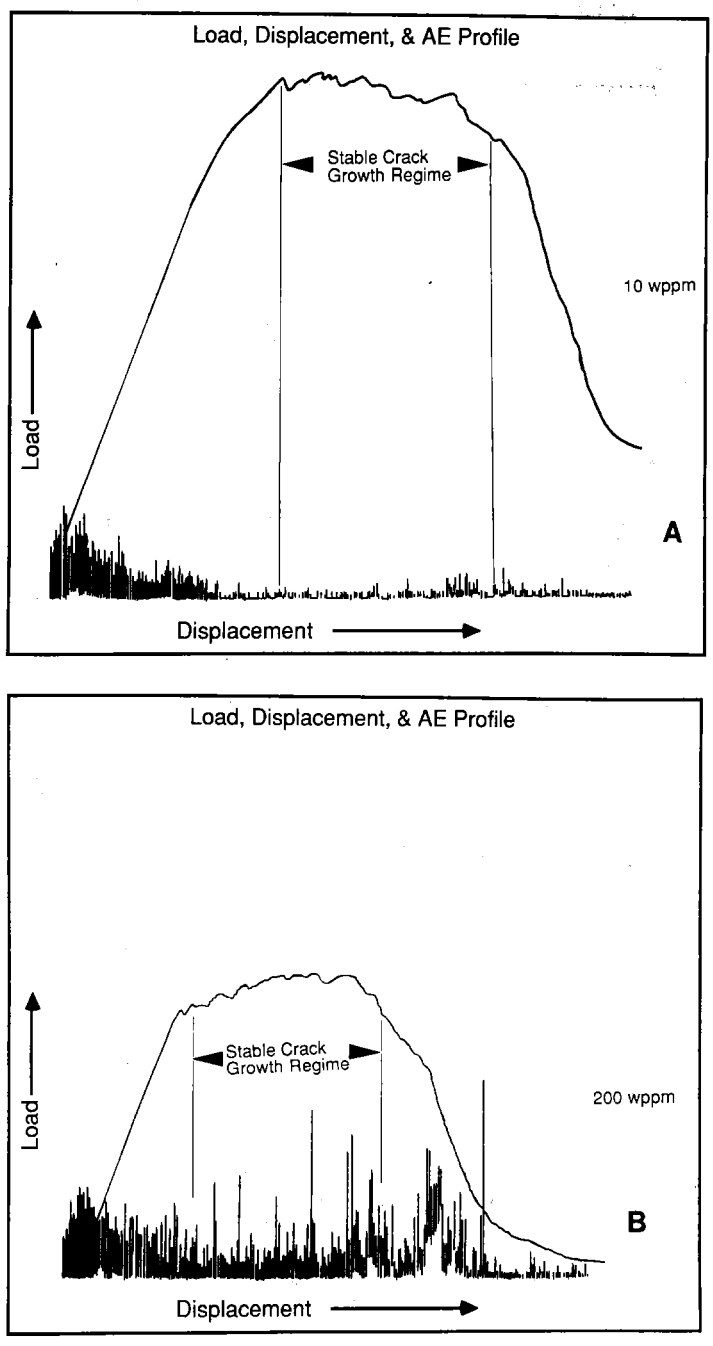

Fig.9: The load/displacement profile is shown coincident with the AE activity profile for materials containing hydrogen concentrations of (A) 10 wppm and (B) 200 wppm. The AE activity is significantly greater for material enriched with internal hydrogen.

microfracture event was much greater during crack propagation. Moreover, the appreciable difference in AE activity observed suggested that mechanisms governing fracture and/or crack extension mode were dissimilar on a local scale despite fracture surface morphological evidence suggesting otherwise. AE results have been used with considerable success elsewhere [20-23] in assessing microfracture mechanisms associated with threshold stress intensity and fracture toughness in several classes of materials. Using AE generated by crack growth, Kishi [20] proposed that the average crack size (pop-in) during fracture toughness testing was approximately equivalent to the unit area defined by prior beta boundaries in Ti-6Al-4V. The association of AE activity with microfracture characteristics was demonstrated also by Nozue and Kishi [21] for 4340 steel heat treated to give a range of fracture toughness values. They showed an increase in AE with decreasing fracture toughness was caused by the increase in the amount of intergranular fracture. In a crack growth study of Ni and several Fe-based alloys in which discontinuous crack growth occurred, Jones, et al., observed that the AE results were correlated to the degree of transgranular fracture accompanying intergranular subcritical cracking. They postulated that AE associated with transgranular fracture was due to ligament failure behind the main crack tip.

Examining the acoustic emission profiles in Figs. 9A and 9B for materials with 10 and 200 wppm hydrogen respectively, one observes that the AE activity was rather high even though the main crack has not initiated in the chevron notch. It was determined that these emissions occurring during loading of the specimen in the elastic region (see Figs. 9A and 9B) were due to stretching and microcrack formation in the tip area of the chevron notch ligament in this titanium alloy. Independent of hydrogen concentration, microcracking occurred at the notch tip prior to initiation of the main crack. Figure 10 shows microcracking at the notch tip that was common to all test specimens. It appeared that the microcracks propagated a short distance (~10-50 microns) along the α/β interface prior to main crack initiation. Presumably, emission sources in this region were hydride cracking along the α/β interface and in the α phase. It is also believed that some of the emissions were attributable to α-case cracking. Alpha (α) case is the nitrogen, oxygen or carbon enriched α stabilized surface resulting from elevated temperature exposure. Apparently, the α-case formed along the edge of the chevron notch during electro-spark discharge machining (EDM) of short bar specimens. Evidence of α-case fracture is shown in Figs. 11A and 11B. Alpha case fracture is revealed by a 50-micron wide band of brittle fracture along the edge of the machined notch in both H-lean, 10 wppm (Fig. 11A) and H-enriched, 200 wppm (Fig. 11B) Ti-6Al-4V samples.

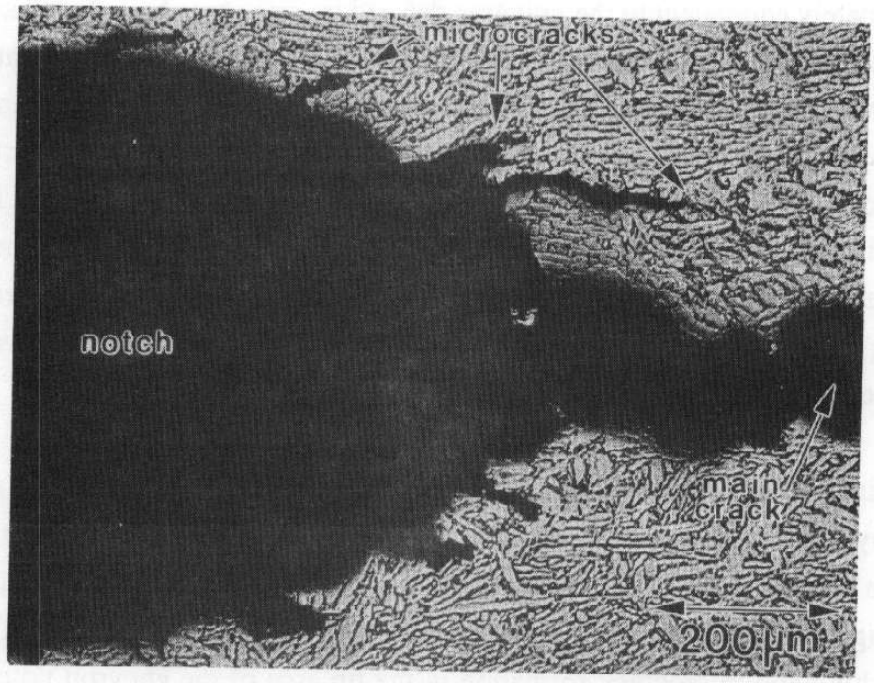

Fig. 10: The notch area is shown for a CNSB specimen. A considerable degree of microcracking is observed prior to initiation of the main crack.

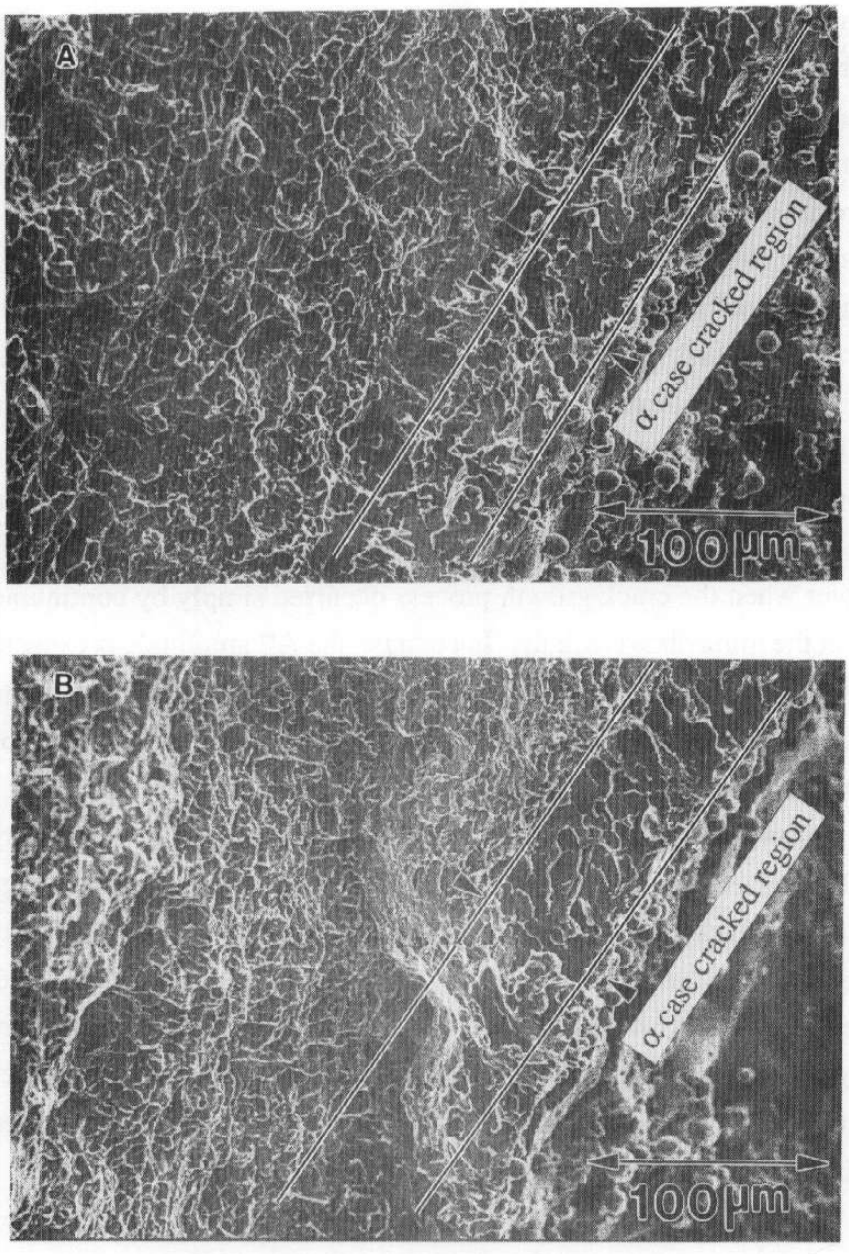

Fig. 11: Alpha case cracking occurred in all test specimens. The α-case cracking is demonstrated by brittle fracture of α platelets in a ~50-micron wide band of material along the edge of the EDM-fabricated chevron notch; (A) 10 wppm and (B) 200 wppm.

While a common emission profile was recognized in the elastic region for all test specimens, such was not the case for the AE activity profile noted in the stable crack growth (SCG) regime where the fracture of the materials is determined (e.g. Figs. 9A and 9B). In the SCG region, high amplitude burst emissions were observed for materials containing high hydrogen concentrations. AE studies on other materials have shown large burst emissions to be associated with fracturing of matrix particles [17,24] and plastic zone expansion [25]. Furthermore, there appeared to be a direct correlation between AE activity and the size of the source responsible for the emissions [18, 20-22]. The high amplitude burst emissions of hydrogen-enriched, low fracture toughness material were thought to be caused by the fracture of ligaments resulting from hydrogen-induced discontinuous growth in the crack tip region. Figures 12A and 12B show the crack tip areas of fracture toughness specimens containing 10 and 200 wppm respectively. Discontinuous crack growth was observed for Ti-6Al-4V alloy with 200 wppm hydrogen and continuous crack growth was exhibited for this alloy containing 10 wppm hydrogen. The micro fracture behavior occurring at the crack tip is commensurate with the AE output profile. That is, one would expect the acoustic emission rate and amplitude to be lower when the crack growth process occurred simply by continuous ductile fracture of material at the immediate crack tip. In contrast, the AE amplitude is expected to be significantly greater when the crack growth process proceeds by discontinuous fracture at the crack tip. Discontinuous crack growth produces a partially fractured zone (semi-cohesive zone) behind the main crack plastic zone. A schematic drawing of a crack tip with a semi-cohesive zone region is shown in Figure 13. It is proposed that the robust AE activity of high H-content material resulted from the fracture of the semi-cohesive zone ligaments formed by discontinuous crack growth. The crack tip metallography and AE activity evidence, strongly supported the contention that the local microfracture mechanisms of hydrogen-enriched and hydrogen-lean Ti-6Al-4V alloys were different. Based on acoustic emission activity and metallographical evidence at the crack tip, it is concluded that fracture occurred by a discontinuous growth process in material enriched with internal hydrogen and by continuous growth in Ti-6Al-4V alloy lean in internal hydrogen content.

Summary and Conclusions

1. Strength and ductility for Ti-6Al-4V alloy were not affected significantly by hydrogen concentration in the range investigated.
2. Reproducible fracture toughness results were obtained by using small CNSB specimens; thus, indicating the usefulness of the short bar test method in determining fracture properties changes.

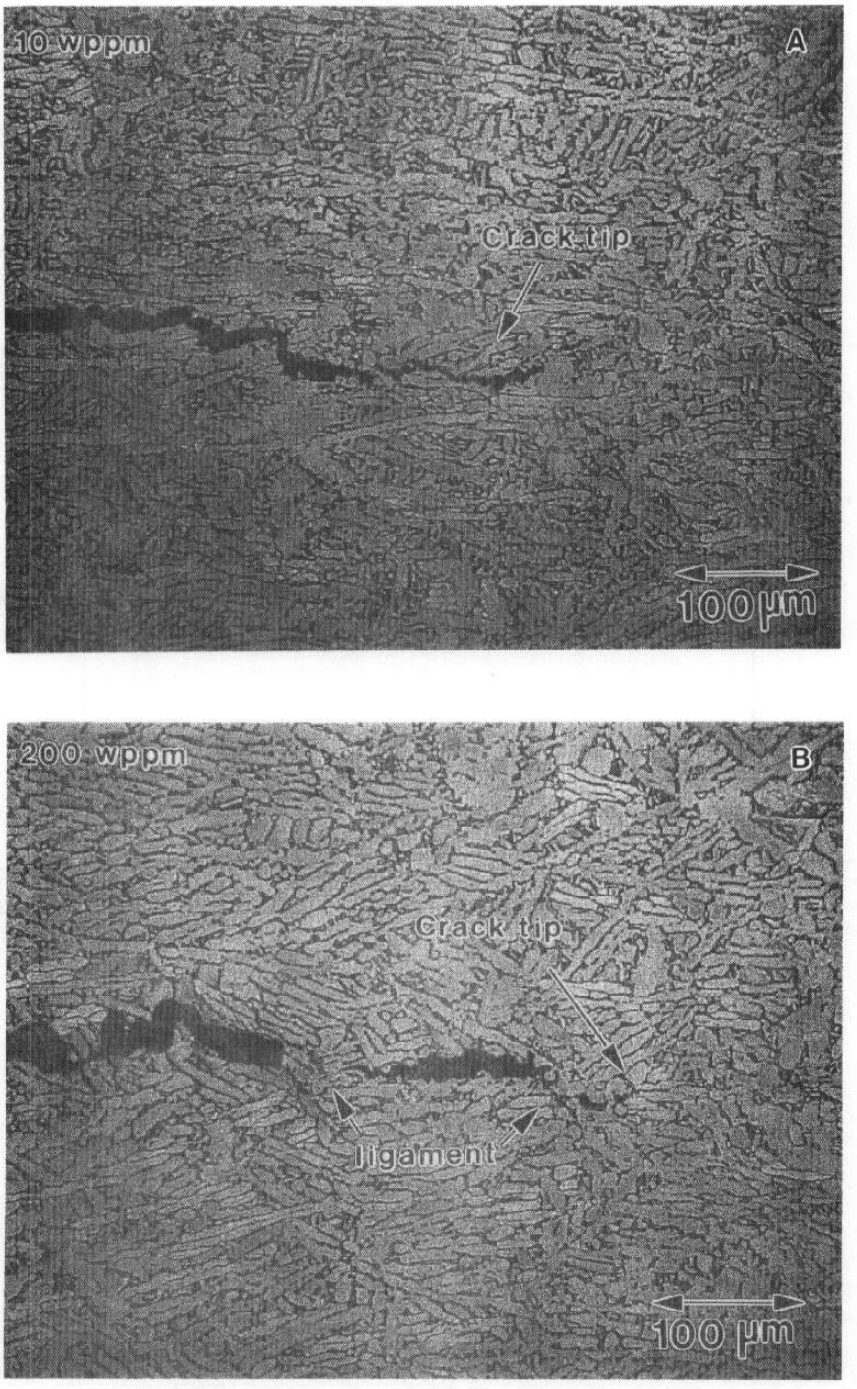

Fig. 12: Crack propagation character at the crack tip region is shown for hydrogen-lean and hydrogen enriched Ti-6Al-4V alloys; (A) continuous crack growth at the crack tip for 10 wppm and (B) discontinuous crack growth at the crack tip for 200 wppm hydrogen.

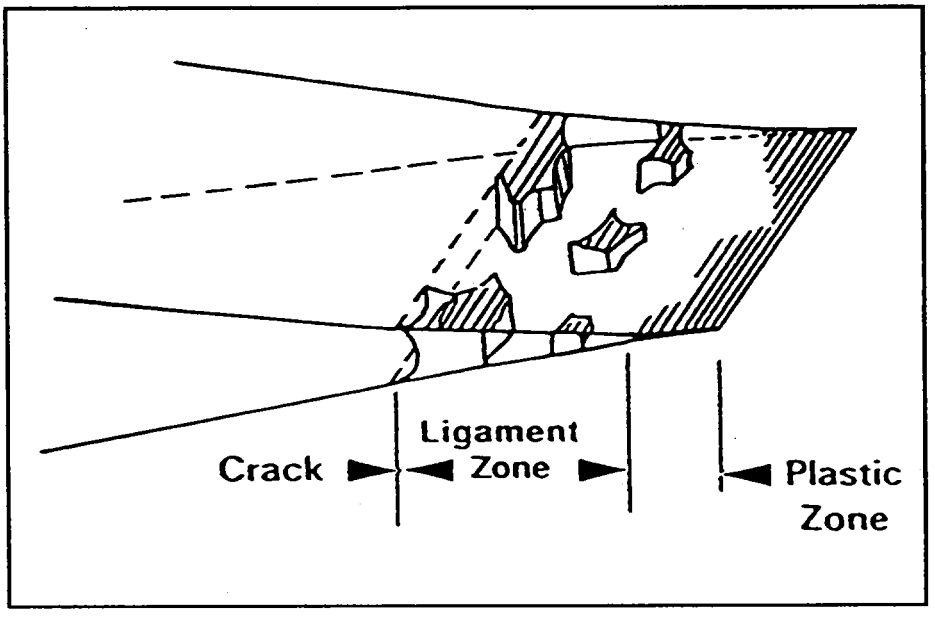

Fig. 13: A model is shown depicting discontinuous crack growth in the crack tip region of materials. In a discontinuous crack growth process, ligaments are left behind the main crack front.

3. The fracture toughness exhibited a marked dependence on hydrogen concentration. At low hydrogen concentrations, fracture toughness results were significantly greater than they were at higher hydrogen concentrations. At high hydrogen concentration, K_{ICSB} values appeared to approach a lower limit.
4. The appreciable change in fracture toughness with hydrogen concentration was not reflected by a commensurate change in fracture surface morphology of Ti-6Al-4V alloy. However, AE results suggested microfracture processes were dissimilar in Ti-6Al-4V alloy of low and high hydrogen concentration levels.
5. Metallographic and AE results indicated that fracture occurred by a discontinuous growth process in hydrogen-rich materials and by a continuous growth process in hydrogen-lean materials.

References

1. H. Hoeg, B. Hollund and I. W. Hall, Metal Science, 4, p. 50 (1980).
2. T. Enjo and T. Kuroda, Trans of JWRI, 13 no. 2, p. 47 (1984).
3. D. N. Williams, F. R. Schwartz and R. I. Jaffe, Trans ASM, 51, p. 802 (1959).
4. R. I. Jaffe and D. N. Williams, Trans ASM, 51, p. 820 (1959).
5. D. N. Williams, J. Inst. Metal, 91, p. 147 (1963).
6. N. Paton and J. C. Williams, "Hydrogen in Metals" (Ed. I. M. Bernstein and A. W. Thompson) p. 409 (1974).
7. H. Margolin, Met. Tran., 7, p. 1233 (1976).
8. D. A. Meyn, Metallurgical Transactions, 5, p. 2405 (1974).
9. D. N. Williams, Met. Trans. 5, p. 2351 (1974).
10. K. Peterson, J. Schwanabeck and W.W. Gerberich, Metallurgical Transactions, 9A, p. 1169 (1978).
11. L. M. Barker, Engineering Fracture Mechanics, 9, p. 361 (1977).
12. L. M. Barker, International Journal of Fracture, 15, p. 515 (1979).
13. P. S. Pao and J. E. O'Neal, Journal of Nuclear Materials, 122 and 123, p. 1587 (1984).
14. D. N. Williams, Materials Science and Engineering, 24, p. 53 (1976).
15. A. Vassel, Journal of the Less Common Metals, 69, p. 293 (1980).
16. J. P. Lucas, "Fracture Toughness and Tensile Properties of H-Charged Ti-6Al-4V" presented at the TMS Meeting Orlando, FL (1986).
17. H. N. G. Wadley, C.B. Scruby and J. H. Speake, International Metals Reviews, Review no. 249, p. 41 (1980).

18. W. W. Gerberich, D. G. Atteridge and L. F. Lessar, Metallurgical Transactions, 6A, p. 797 (1975).
19. J. D. Desai and W. W. Gerberich, Engineering Fracture Mechanics, 7, p. 153 (1975).
20. T. Kishi, H. S. Park, R. Horiuchi, T. Kamkimi, M. Nakanose and T. Tanabe, "Titanium '80 Science and Technology" (Ed. H. Kimura and O. Izumi) p. 1709 (1980).
21. A. Nozue and T. Kishi, Journal of Acoustic Emission, 1, p. 1 (1982).
22. R. H. Jones, M. A. Freisel, and W. W. Gerberich, Metallurgical Transactions, 20A, p. 637 (1989).
23. J. C. Radon and A. A. Pollock, Eng. Frac. Mech., 4, p. 295 (1972).
24. M. A. Hamstad, R. Bianchetti and A. K. Mukherjee, Eng. Frac. Mech., 11, p. 663 (1977).
25. I. G. Palmer and P. T. Heald, Mat. Sci. and Eng., 11, p. 181 (1973).

UNLIMITED RELEASE

INITIAL DISTRIBUTION

W. W. Gerberich
University of Minnesota
Dept. of Chemical Engineering
and Materials Science
421 Washington Avenue, SE
Minneapolis, MN 55455

R. O. Ritchie
Dept. of Materials Science
and Mineral Engineering
Hearst Mining Building
Berkeley, CA 94720

K. R. Brown
Aluminum & Chemical Corporation
Center for Technology
P.O. Box 877
Pleasanton, CA 94566

Toby M. Cordell
Structural Composites
Structural Materials Branch
AFWAL/MLBC
Wright-Patterson AFB
Dayton, OH 45433-6533

Christopher F. Johnson
Terra Tek Systems
University Research Park
#60 Wakara Way
Salt Lake City, UT 84108

A. W. Thompson
Carnegie-Mellon University
Dept. of Metallurgy and Mat. Sci.
Schenley Park
Pittsburgh, PA 15213

R. H. Jones
Battelle Pacific Northwest
P.O. Box 999
Richland, WA 99252

R. R. Boyer
Doeing Commercial Airplane Co.
P.O. Box 3707, MS 73-43
Seattle, WA 98124

M. R. Louthan
Westinghouse
Savannah River Site
Aiken, SC 29801-0001

D. A. Meyn
Naval Research Laboratory
Code 6312
Materials Science
and Technology Division
Washington, DC 20375

M. Morgan
Westinghouse
Savannah River Site
Aiken, SC 29801-0001

Dr. Neil Paton
Rockwell International
Rocketdyne
6633 Canoga Ave. AL17
Canoga Park, CA 91303-2790

G. R. Yoder
Naval Research Laboratory
Materials Science and
Technology Division
Washington, DC 29808

H. J. Rack
Dept. of Mechanical Engineering
Riggs Hall
Clemson University
Clemson, SC 29634-0921

H. G. Nelson
Ames Research Center
NASA Ames N230-4
Moffett Field, CA 94035

K. V. Jata
University of Dayton Research Inst.
300 College Park Dr.
Dayton, OH 45469

W. M. Garrison
Carnegie-Mellon University
Dept. of Metallurgy and Mat. Sci.
Schenley Park
Pittsburgh, PA 15213

A. K. Muhkerjee
Dept. of Mechanical Engineering
University of California
Davis, CA 95617

Lawrence Livermore National Laboratory
R. Riddle L342

1534 L. M. Barker
1800 R. J. Eagan
Attn: D. W. Schaefer, 1810
J. B. Woodard, 1820
M. J. Davis, 1830
R. E. Loehman, 1840
1831 A. D. Romig
1832 W. B. Jones
1832 J. A. Van Den Avyle
7470 J. L. Ledman
7472 J. A. Sayre

8000 J. C. Crawford
Attn: E. E. Ives, 8100
R. J. Detry, 8200
R. C. Wayne, 8400
P. E. Brewer, 8500
8165 G. C. Story
8300 P. L. Mattern
Attn: W. Bauer, 8340
J. S. Binkley, 8350
W. J. McLean, 8360
8310 P. L. Mattern, Acting
Attn: D. L. Lindner, 8311
J. M. Hruby, 8313
M. W. Perra, 8314
R. E. Stoltz, 8316
8311 J. R. Spingarn
8312 M. I. Baskes
8312 J. A. Brooks
8312 J. P. Lucas (5)
8312 N. R. Moody
8312 B. C. Odegard
8314 M. J. Mills
8314 S. L. Robinson
8316 J. E. Costa

8535 Publications/Technical Library Processes, 3141
3141 Technical Library Processes Division (3)
8524-2 Central Technical Files (3)

8232-2/069868

00000002 -

8232-2/069868

00000002 -

8232-2/069868

00000002 -

Org.	Bldg.	Name	Rec'd by	Org.	Bldg.	Name	Rec'd by

Sandia National Laboratories